ISSN 1392-1207. MECHANIKA. Vol. 29, No. 6, 2023: 454–461

Effect of Surface Elastic Deformation in Hydrodynamic Inclined Fixed Pad Thrust Bearing with Low Clearance

Jinxin ZHU, Yongbin ZHANG
College of Mechanical Engineering, Changzhou University, Changzhou, Jiangsu Province, China,
E-mails: yongbinzhang@cczu.edu.cn, engmech1@sina.com (Corresponding Author)

https://doi.org/10.5755/j02.mech.33803

1. Introduction

Hydrodynamic thrust slider bearings have been theoretically studied plentifully by considering non-Newtonian fluids, surface roughness, fluid film viscous heating and surface elastic deformation [1-8]. Those studies addressed the bearing clearances over 0.1 μm, which is normally far larger than the thickness of the physically adsorbed layer on the bearing surface. In such bearings, the effect of the adsorbed layer is negligible and the case fits a lot of practical operating conditions. However, in the condition of heavy loads and high sliding speeds, the clearance of the hydrodynamic slider bearing can be as low as on the same scale with the adsorbed layer thickness owing to the severe frictional heating [9]. For this case, the effect of the adsorbed layer must be considered. In reduced-size bearings, even for moderate loads and sliding speeds, the bearing clearance is comparable to the adsorbed layer thickness. Obviously, in these bearings the adsorbed layer effect should also be considered. There is the multiscale hydrodynamic regime in the bearing where the sandwich film occurs consisting of both the adsorbed layer and the intermediate continuum fluid [10-12].

How to consider the effect of the adsorbed layer in a multiscale hydrodynamic contact is challenging. One computational method is to simulate the adsorbed layer flow by molecular dynamics simulation while to simulate the intermediate continuum fluid flow by the Newtonian fluid model [13-15]. This method is currently applicable for the contact size no more than hundreds nanometers, however is difficult to use for bigger contact sizes because of over cost of computational time and computer storage. The simplest method is to treat the adsorbed layer as an immobile solid layer and treat the intermediate fluid as a continuum fluid [16]. It is applicable when the fluid-bearing surface interaction is so strong that the adsorbed layer is highly solidified. However, in a general case, the adsorbed layer should be treated as a flowing layer. Zhang has developed the closed-form explicit multiscale flow equations for both the adsorbed layer flow and the intermediate continuum fluid flow for the two-dimensional flow (with the side leakage neglected) [10]. The advantage of his approach is high computational efficiency capable of solving engineering multiscale flow problems with very wide contact sizes just by using currently normal computers.

Huang et al. [12] analytically derived the mathematical equations respectively for calculating the film pressure and carried load of the hydrodynamic inclined fixed pad thrust slider bearing with low clearances considering both the flows of the adsorbed layer and the intermediate continuum fluid, by using Zhang's equation and treating the bearing surfaces as rigid. Their calculation results show the significant improvement of the load-carrying capacity of the bearing by the adsorbed layer effect especially when the fluid-bearing surface interaction is strong.

Surface elastic deformation was usually neglected in the previous studies on hydrodynamic thrust slider bearings because of the low film pressures [1-6]. There are also some literatures on the surface elastic deformation effect in a hydrodynamic slider bearing without considering the effect of the adsorbed layer [7, 8]. In the multiscale hydrodynamic thrust slider bearing as described above, because of the low clearance and the effect of the adsorbed layer, the generated film pressures can be much higher than those in the classical bearing and they may cause the elastic deformations of the bearing surfaces comparable to and even larger than the bearing clearance. It appears necessary to further address the effect of surface elastic deformation in the multiscale hydrodynamic inclined fixed pad thrust slider bearing. The present paper attempts to do this work. The surface elastic deformation effect was found to be pronounced and it reduces the load-carrying capacity of the bearing especially for a strong fluid-bearing surface interaction.

2. Studied bearing

Fig. 1 shows the studied multiscale hydrodynamic inclined fixed pad thrust slider bearing with low clearances where the thickness of the physically adsorbed layer on the bearing surface is comparable to the surface separation and there is the continuum fluid film between the two adsorbed layers.

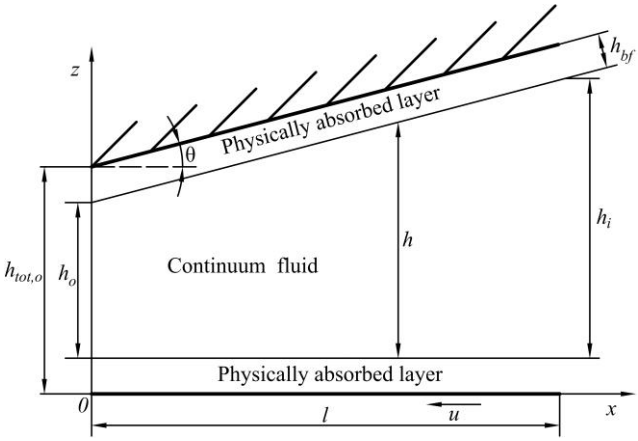

Fig. 1 The studied multiscale hydrodynamic inclined fixed pad thrust slider bearing with low clearance

The upper bearing surface is stationary and the lower bearing surface is moving with the speed u. The two bearing surfaces are steel and the adsorbed layers on them are assumed as identical with the thickness h_{bf}. The tilting angle of the bearing is θ and the bearing width is l. The thickness of the intermediate continuum fluid film is h, and its values on the entrance and exit of the bearing are respectively h_i and h_o. The surface separation on the exit of the bearing is $h_{tot,o}$.

3. Analysis

Except the surface elastic deformation calculation, the analysis in the present paper is the same with that by Huang et al. [12] for rigid bearing surfaces. For convenience in understanding, some of them are repeated here.

The present analysis is based on the following assumptions:

1. The flow inertia is neglected;
2. The side leakage is neglected;
3. The film viscous heating effect is neglected;
4. The two bearing surfaces are perfectly smooth;
5. No interfacial slippage occurs on any interface;
6. The condition is steady-state.

For numerical analysis, (N+1) discretized points are evenly distributed in the whole hydrodynamic area of the bearing, as shown in Fig. 2. The distance between two neighboring discretized points is: $\delta_x = l / N$. The x coordinate of the Jth discretized point is: $x_J = J \cdot \delta_x$.

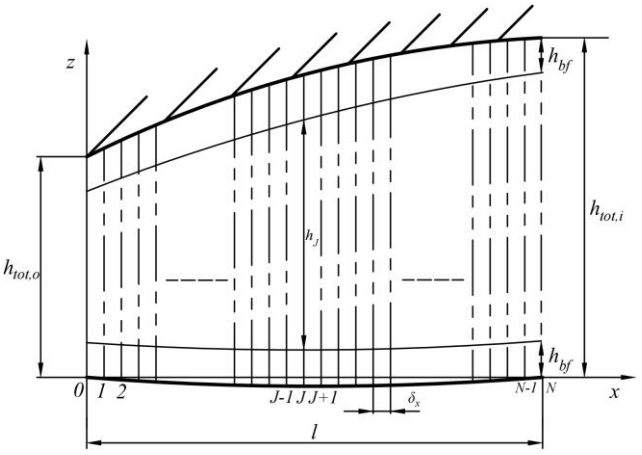

Fig. 2 The studied multiscale hydrodynamic inclined fixed pad thrust slider bearing with low clearance

$$q_m = \left[\frac{F_1 h_{bf}^3}{6\eta_{bf}^{eff}} \frac{\partial p}{\partial x} - \frac{h_{bf}^3}{\eta_{bf}^{eff}} \frac{\partial p}{\partial x} \left(1 + \frac{1}{2\lambda_{bf}} - \frac{q_0 - q_0^n}{q_0^{n-1} - q_0^n} \frac{\Delta_{n-2}}{h_{bf}} \right) \frac{\varepsilon}{1 + \dfrac{\Delta x}{D}} - u h_{bf} \right] \rho_{bf}^{eff} +$$

$$+ \left\{ \frac{h^3}{\eta_{bf}^{eff}} \frac{\partial p}{\partial x} \left[\frac{F_2 \lambda_{bf}^2}{6} - \frac{\lambda_{bf}}{1 + \dfrac{\Delta x}{D}} \left(\frac{1}{2} + \lambda_{bf} - \frac{q_0 - q_0^n}{q_0^{n-1} - q_0^n} \frac{\Delta_{n-2}}{h} \right) \right] - \frac{h^3}{12\eta} \frac{\partial p}{\partial x} - \frac{uh}{2} \right\} \rho, \quad (1)$$

where: $\lambda_{bf} = h_{bf} / h$, p is the hydrodynamic pressure; D is the fluid molecule diameter; x is the coordinate shown in Fig. 1; η_{bf}^{eff} is the effective viscosity of the adsorbed layer, η is the fluid bulk viscosity; ρ_{bf}^{eff} is the average density of the adsorbed layer; ρ is the fluid bulk density; n is the equivalent number of the fluid molecules across the adsorbed layer thickness; Δx is the separation between the neighboring fluid molecules in the x coordinate direction in the adsorbed layer; Δ_{n-2} is the separation between the neighboring fluid molecules across the adsorbed layer thickness just on the boundary between the adsorbed layer and the continuum fluid; $q_0 = \Delta_{j+1}/\Delta_j$ (Δ_j is the separation between the $(j+1)^{\text{th}}$ and j^{th} fluid molecules across the adsorbed layer thickness) and q_0 is the averaged constant $(q_o > 1)$.

$$\varepsilon = \left(2DI + II\right) / \left[h_{bf} \left(n-1\right) \left(\Delta_l / \eta_{line,l} \right)_{avr,n-1} \right], \quad (2)$$

$$F_1 = \eta_{bf}^{eff} \left(12D^2 \Psi + 6D\Phi\right) / h_{bf}^3, \quad (3)$$

$$F_2 = 6\eta_{bf}^{eff} D \left(n-1\right) \left(l\Delta_{l-1} / \eta_{line\ ,l-1} \right)_{avr,n-1} / h_{bf}^2, \quad (4)$$

$$I = \sum_{i=1}^{n-1} i \left(\Delta_l / \eta_{line\ ,l} \right)_{avr,i}, \quad (5)$$

$$\Psi = \sum_{i=1}^{n-1} i \left(l\Delta_{l-1} / \eta_{line,l-1} \right)_{avr,i}, \quad (6)$$

$$II = \sum_{i=0}^{n-2} \left[\begin{matrix} i \left(\Delta_l / \eta_{line\ ,l} \right)_{avr,i} \\ + \left(i+1\right) \left(\Delta_l / \eta_{line,l} \right)_{avr,i+1} \end{matrix} \right] \Delta_l, \quad (7)$$

$$\Phi = \sum_{i=0}^{n-2} \left[\begin{matrix} i \left(l\Delta_{l-1} / \eta_{\text{line}\ ,l-1} \right)_{avr,i} \\ + \left(i+1\right) \left(l\Delta_{l-1} / \eta_{line\ ,l-1} \right)_{avr,i+1} \end{matrix} \right] \Delta_l, \quad (8)$$

$$i \left(\Delta_l / \eta_{line,l} \right)_{avr,i} = \sum_{j=1}^{i} \Delta_{j-1} / \eta_{line\ ,j-1}, \quad (9)$$

$$i \left(l\Delta_{l-1} / \eta_{line\ ,l-1} \right)_{avr,i} = \sum_{j=1}^{i} j\Delta_{j-1} / \eta_{line\ ,j-1}, \quad (10)$$

where: $\eta_{line,j-1}$ is the local viscosity between the j^{th} and $(j-1)^{\text{th}}$ fluid molecules across the adsorbed layer thickness, and it was assumed that $\eta_{line,j} / \eta_{line,j+1} = q_0^{\gamma}$.

The fluid viscosity is expressed by the Roelands equation:

$$\eta = \eta_a exp \left\{ \left(ln\eta_a + 9.67 \right) \left[\left(1 + p \cdot 5.1\text{E}-9 \right)^G - 1 \right] \right\}, \quad (11)$$

where: $G=\zeta/\left[(5.1\mathrm{E}-9)(ln\eta_a+9.67)\right]$; η_a is the fluid viscosity at atmospheric pressure, and ζ is constant. The fluid density is expressed as: $\rho=\rho_a(1+\beta\cdot p)$ where ρ_a is the fluid density at atmospheric pressure and β is constant.

Considering the elastic deformations of both the bearing surfaces, the surface separation on the J^{th} discretized point is formulated as:

$$h_{tot,J}=h_{oo}+x_J tan\theta-\frac{2}{\pi E_v}\int_0^l p(s)ln\left(x_J-s\right)^2 ds, \quad (12)$$

where h_{oo} is constant and E_v is the compound Young's modulus of elasticity of two bearing surfaces.

The thickness of the intermediate continuum fluid film on the J^{th} discretized point is then:

$$h_J=h_{oo}+x_J tan\theta-\frac{2}{\pi E_v}\int_0^l p(s)ln\left(x_J-s\right)^2 ds-2h_{bf}. \quad (13)$$

According to Eqs.(1) and (13), the pressure gradient on the J^{th} discretized point is written as:

$$\left.\frac{dp}{dx}\right|_J=\frac{u\rho_J\left[h_{oo}+x_J tan\theta-\frac{2}{\pi E_v}\int_0^l p(s)ln\left(x_J-s\right)^2 ds-2h_{bf}\right]+2q_m+2uh_{bf}\rho_{bf,J}^{eff}}{\frac{2c\rho_J\left[h_{oo}+x_J tan\theta-\frac{2}{\pi E_v}\int_0^l p(s)ln\left(x_J-s\right)^2 ds-2h_{bf}\right]^3}{\eta_J}+\frac{2d\rho_{bf,J}^{eff}h_{bf}^3}{\eta_{bf,J}^{eff}}}, \quad (14)$$

where:

$$c=\frac{1}{C_y}\left[\frac{F_2\lambda_{bf}^2}{6}-\frac{\lambda_{bf}}{1+\frac{\Delta x}{D}}\left(\frac{1}{2}+\lambda_{bf}-\frac{q_0-q_0^n}{q_0^{n-1}-q_0^n}\frac{\Delta_{n-2}\lambda_{bf}}{h_{bf}}\right)\right]-\frac{1}{12}, \quad (15)$$

$$\eta_{bf,J}^{eff}=C_y\cdot\eta_J=$$
$$=C_y\cdot\eta_a exp\left\{\left(ln\eta_a+9.67\right)\left[\left(1+p_{J-1}\cdot 5.1\mathrm{E}-9\right)^G-1\right]\right\}, \quad (16)$$

$$d=\frac{F_1}{6}-\left(1+\frac{1}{2\lambda_{bf}}-\frac{q_0-q_0^n}{q_0^{n-1}-q_0^n}\frac{\Delta_{n-2}}{h_{bf}}\right)\frac{\varepsilon}{1+\frac{\Delta x}{D}}, \quad (17)$$

$$\rho_{bf,J}^{eff}=C_q\cdot\rho_J=C_q\cdot\rho_a\left(1+\beta p_{J-1}\right). \quad (18)$$

Here, η_J and ρ_J are respectively the fluid viscosity and density on the J^{th} discretized points; $\eta_{bf,J}^{eff}$ and $\rho_{bf,J}^{eff}$ are respectively the effective viscosity and average density of the adsorbed layer on the J^{th} discretized points.

By forward difference, it is expressed that:

$$\left.\frac{dp}{dx}\right|_J=\frac{p_J-p_{J-1}}{\delta_x}, \text{ for } J=1, 2, 3,\ldots, N, \quad (19)$$

where: p_J and p_{J-1} are respectively the pressures on the J^{th} and $(J\text{-}1)^{\text{th}}$ discretized points.

The pressure on the J^{th} discretized point is easily written as:

$$p_J=\sum_{K=1}^{J}\left(p_K-p_{K-1}\right)+p_0, \text{ for } J=1, 2, 3,\ldots, N. \quad (20)$$

The boundary condition gives that $p_0=0$ Substituting Eq. (14) into Eq. (19) and further substituting Eq. (19) into Eq. (20) thus gives that:

$$p_J=\frac{l}{N}\sum_{K=1}^{J}\frac{u\rho_K\left(h_{oo}+x_K tan\theta-\frac{2}{\pi E_v}\int_0^l p(s)ln\left(x_K-s\right)^2 ds-2h_{bf}\right)+2q_m+2uh_{bf}\rho_{bf,K}^{eff}}{\frac{2c\rho_K\left[h_{oo}+x_K tan\theta-\frac{2}{\pi E_v}\int_0^l p(s)ln\left(x_K-s\right)^2 ds-2h_{bf}\right]^3}{\eta_K}+\frac{2d\rho_{bf,K}^{eff}h_{bf}^3}{\eta_{bf,K}^{eff}}}, \text{ for } J=1, 2, 3, \ldots, N. \quad (21)$$

The load per unit contact length carried by the bearing is:

$$w=\int_0^l pdx=\left(\frac{l}{N}\right)^2\sum_{J=1}^{N}\left(\sum_{K=1}^{J}\frac{u\rho_K\left(h_{oo}+x_K tan\theta-\frac{2}{\pi E_v}\int_0^l p(s)ln\left(x_K-s\right)^2 ds-2h_{bf}\right)+2q_m+2uh_{bf}\rho_{bf,K}^{eff}}{\frac{2c\rho_K\left(h_{oo}+x_K tan\theta-\frac{2}{\pi E_v}\int_0^l p(s)ln\left(x_K-s\right)^2 ds-2h_{bf}\right)^3}{\eta_K}+\frac{2d\rho_{bf,K}^{eff}h_{bf}^3}{\eta_{bf,K}^{eff}}}\right). \quad (22)$$

4. Calculation

4.1. Numerical integration

In the surface elastic deformation calculation, there is the following term (Eq. (13)):

$$\Theta_J = -\frac{2}{\pi E_v}\int_0^l p(s)\ln\left(x_J - s\right)^2 ds. \tag{23}$$

Since $p(s)$ cannot be exactly formulated, the integration in Eq. (23) is generally numerically calculated by interpolating $p(s)$ according to the pressure values on the discretized points. Thus, Eq. (23) is approximately expressed as:

$$\Theta_J \approx \sum_{I=1}^{N-1} K_{JI}\, p_I\,, \tag{24}$$

where:

$$K_{JI} = -\frac{2}{\pi E_v}\int_{\frac{x_I + x_{I-1}}{2}}^{\frac{x_I + x_{I+1}}{2}} \ln\left(x_J - s\right)^2 ds. \tag{25}$$

Here, x_{I-1}, x_I and x_{I+1} are respectively the x coordinates of the $(I\text{-}1)^{\text{th}}$, I^{th} and $(I\text{+}1)^{\text{th}}$ discretized points. It is then found that:

$$\begin{aligned} K_{JI} = &-\frac{2}{\pi E_v}\ln\left(\frac{x_I + x_{I+1}}{2} - x_J\right)^2\left(\frac{x_I + x_{I+1}}{2} - x_J\right) + \\ &+\frac{2}{\pi E_v}\ln\left(\frac{x_I + x_{I-1}}{2} - x_J\right)^2\left(\frac{x_I + x_{I-1}}{2} - x_J\right) + \\ &+\frac{2}{\pi E_v}\left(x_{I+1} - x_{I-1}\right). \end{aligned} \tag{26}$$

4.2. Numerical solution procedure

The present studied problem is highly non-linear and the solution can only be numerically found. Fig. 3 shows the numerical solution procedure. k is the iteration order number; $p^{(0)}$, $h^{(0)}$, and $w^{(0)}$ are respectively the hydrodynamic pressure distribution, continuum film thickness distribution and bearing load for rigid surfaces; $h_{tot,o,r}$ is the surface separation on the exit of the bearing for rigid surfaces. It is satisfied that $h_{oo,min} \le h_{oo} \le h_{oo,max}$; $\Theta^{(k)}$ is the value of Θ in the k^{th} iteration; $p^{(k)}$ is the hydrodynamic pressure value in the k^{th} iteration; $h^{(k)}$ is the value of h in the k^{th} iteration; ϑ is the relaxation factor; $w_{max}^{(1)}$ and $w_{mid}^{(1)}$ are respectively the calculated bearing loads for elastic surfaces when $h_{oo} = h_{oo,max}$ and $h_{oo} = h_{oo,mid}$; $Q_m^{(k+1)}$ is the dimensionless mass flow rate per unit contact length through the bearing obtained in the $(k\text{+}1)^{\text{th}}$ iteration and it is satisfied that $Q_{m,min}^{(k+1)} \le Q_m^{(k+1)} \le Q_{m,max}^{(k+1)}$. Here, it is defined that $Q_m = q_m / u\rho_a h_{tot,o}$. Then, the pressures on all the discretized points can be calculated from the equations shown above, by starting the calculation from the exit of the bearing. $p_{N,min}^{(k+1),0}$ and $p_{N,m}^{(k+1),0}$ are respectively the hydrodynamic pressures on the entrance of the bearing when $Q_m^{(k+1)} = Q_{m,min}^{(k+1)}$ and $Q_m^{(k+1)} = (Q_{m,min}^{(k+1)} + Q_{m,max}^{(k+1)})/2$. The value of Q_m will be obtained when the following convergence criterion is satisfied:

$$2\left|\left(Q_{m,max}^{(k+1)} - Q_{m,min}^{(k+1)}\right) / \left(Q_{m,max}^{(k+1)} + Q_{m,min}^{(k+1)}\right)\right| < 0.1\%\,.$$

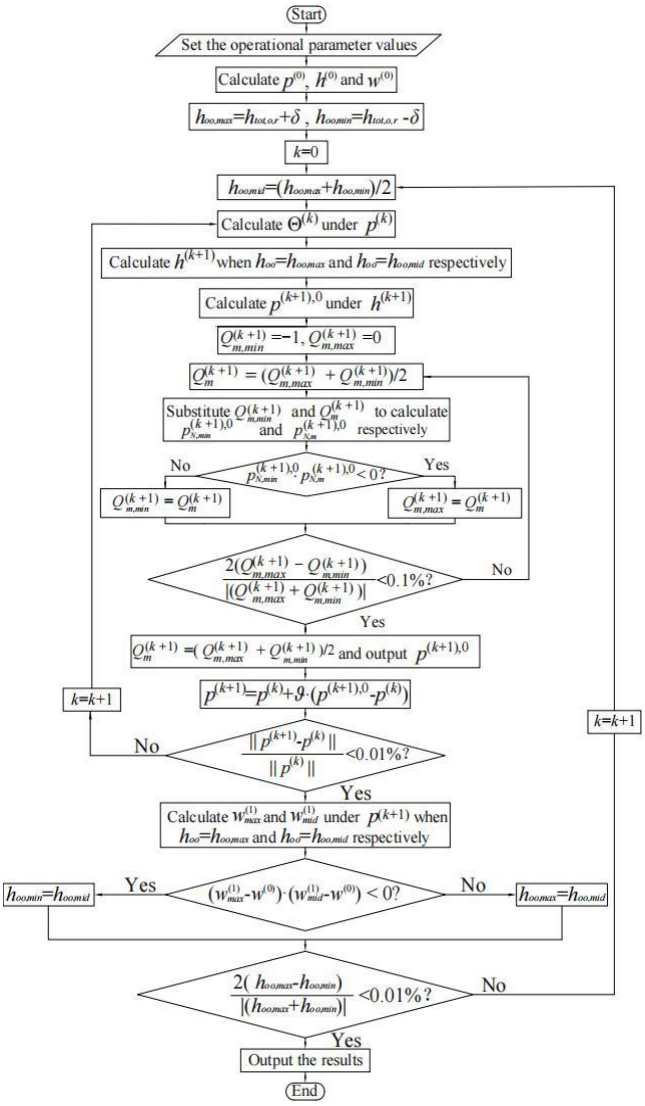

Fig. 3 The numerical solution procedure

4.3. Parameter formulations

The parameter C_q is expressed as [16]:

$$C_q\left(H_{bf}\right) = \begin{cases} 1, & \text{for } H_{bf} \ge 1 \\ m_0 + m_1 H_{bf} + m_2 H_{bf}^2 + m_3 H_{bf}^3, & \text{for } 0 < H_{bf} < 1 \end{cases} \tag{27}$$

where: $H_{bf} = h_{bf} / h_{cr,bf}$, $h_{cr,bf}$ is the critical thickness for characterizing the rheological properties of the adsorbed layer, and m_0, m_1, m_2 and m_3 are respectively constant.

The parameter C_y is expressed as [16]:

$$C_y\left(H_{bf}\right)=\begin{cases}1, & \text{for } H_{bf}\geq 1\\ a_0+\dfrac{a_1}{H_{bf}}+\dfrac{a_2}{H_{bf}^2}, & \text{for } 0<H_{bf}<1'\end{cases} \quad (28)$$

where: a_0, a_1 and a_2 are respectively constant.

The parameters F_1, F_2 and ε have been respectively regressed out as [10]:

$$F_1=0.18\left(\frac{\Delta_{n-2}}{D}-1.905\right)\left(lnn-7.897\right), \quad (29)$$

$$F_2=-\left(3.707\text{E}-4\right)\left(\frac{\Delta_{n-2}}{D}-1.99\right)\left(n+64\right)\cdot \cdot\left(q_0+0.19\right)\left(\gamma+42.43\right), \quad (30)$$

and

$$\varepsilon=\left(4.56\text{E}-6\right)\left(\frac{\Delta_{n-2}}{D}+31.419\right)\left(n+133.8\right)\cdot \cdot\left(q_0+0.188\right)\left(\gamma+41.62\right). \quad (31)$$

The thickness of the adsorbed layer was calculated as:

$$h_{bf}=nD+\Delta_{n-2}\frac{q_0-q_0^n}{q_0^{n-1}-q_0^n}. \quad (32)$$

In the calculations, it was taken that: D = 0.5 nm, $\Delta_{n\text{-}2}/D = \Delta x/D$ = 0.15, ϑ = 0.2, $\zeta=\left(1.6\text{E}-8\right)$ m^2 / N, β = 4E-10 Pa^{-1} η_a = 0.03 Pa s, θ = 1E-4 rad, l = 100 μm, E_v = 2.09E11 Pa, $N = 1000\delta$ = 7 nm

The weak, medium and strong fluid-bearing surface interactions were respectively considered. For the weak interaction: $h_{cr,bf}$ = 7 nm γ = 0.5 n = 3, q_0 = 1.05. For the medium interaction: $h_{cr,bf}$ = 20 nm γ = 1.0 n = 5, q_0 = 1.1. For the strong interaction: $h_{cr,bf}$ = 40 nm γ = 1.5 n = 8, q_0 = 1.2. For these three interactions, the values of h_{bf} are respectively 1.65 nm, 2.76 nm and 4.32 nm.

For different fluid-bearing surface interactions, the viscosity and density parameter values for the adsorbed layer are respectively shown in Tables 1 and 2.

Table 1
Fluid viscosity data for different fluid-bearing surface interactions [16]

Parameter / Interaction	a_0	a_1	a_2
Strong	1.8335	-1.4252	0.5917
Medium	1.0822	-0.1758	0.0936
Weak	0.9507	0.0492	1.6447E-4

Table 2
Fluid density data for different fluid-bearing surface interactions [16]

Parameter / Interaction	m_0	m_1	m_2	m_3
Strong	1.43	-1.723	2.641	-1.347
Medium	1.30	-1.065	1.336	-0.571
Weak	1.116	-0.328	0.253	-0.041

5. Results

5.1. Comparison of the surface separations and hydrodynamic pressures calculated respectively for elastic surfaces and rigid surfaces

Fig. 4 compares the surface separations calculated respectively for elastic surfaces and rigid surfaces based on the present multiscale model when w = 500 N/m, u = 1.5E − 3 m/s, and the fluid-bearing surface interaction is respectively weak, medium and strong. They are also compared with those calculated from conventional hydrodynamic lubrication theory [17]. It is shown that the effect of the bearing surface elastic deformation reduces both the minimum and maximum surface separations, which respectively occur on the exit and entrance of the bearing. Owing to the surface elastic deformations, the surface separation profile of the bearing is significantly different from that assumed by the classical theory, which is based on rigid surfaces.

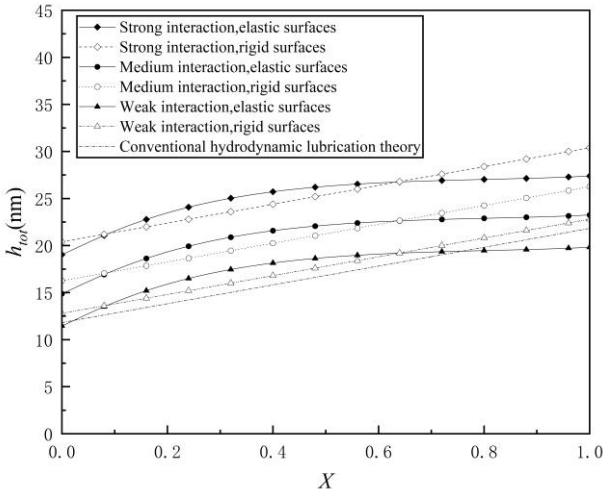

Fig. 4 Comparison between surface separations calculated respectively for elastic surfaces and rigid surfaces based on the present multiscale model and calculated from conventional hydrodynamic lubrication theory when w = 500 N/m and $u = 1.5E-3$ m/s

Figs. 5, a-c show that for given load and sliding speed, owing to the effect of the bearing surface elastic deformations, the maximum pressure in the bearing is increased and its location is moved closer to the exit of the bearing. These effects are more significant for a stronger fluid-bearing surface interaction.

Fig. 6 shows that when both the minimum surface separation $h_{tot,min}$ and the sliding speed u are fixed, owing to the effect of the surface elastic deformations, the surface separation profile more significantly deviates from the classical result when the fluid-bearing surface interaction is stronger.

Fig. 7 shows that for given $h_{tot,min}$ and u, owing to the effect of the surface elastic deformations, most of the hydrodynamic pressures including the maximum pressure in the bearing are significantly reduced especially for a strong fluid-bearing surface interaction. However, for a weak fluid-bearing surface interaction, this effect is weak.

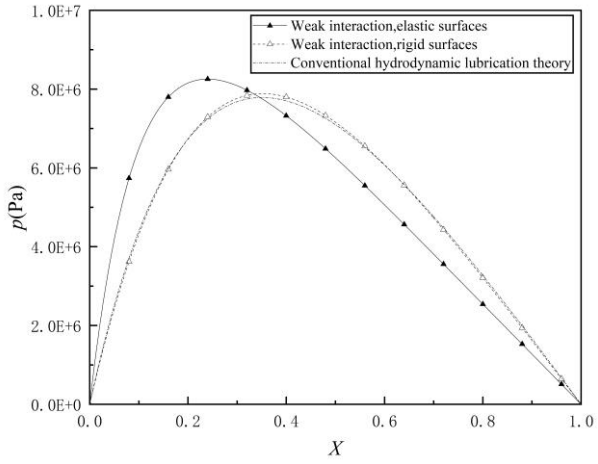

a) For the weak interaction

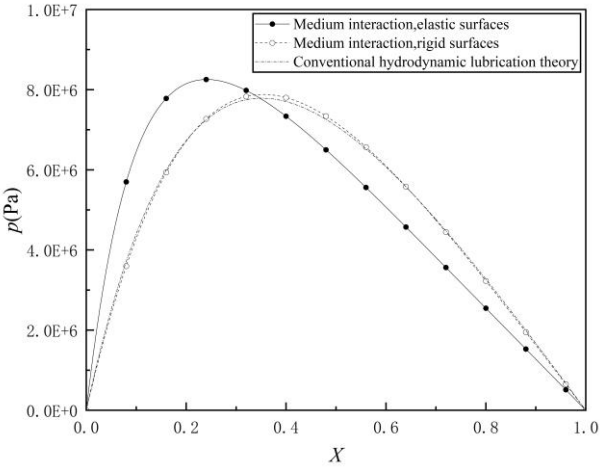

b) For the medium interaction

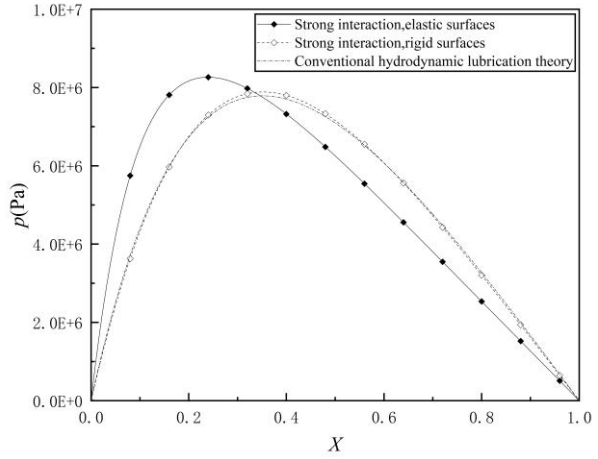

c) For the strong interaction

Fig. 5 Comparison of the hydrodynamic pressure distributions calculated respectively for elastic surface and rigid surface based on the present multiscale model when w = 500 N/m and u = 1.5E-3 m/s

5.2. Comparison of the load (W) versus minimum surface separation ($h_{tot,min}$) curves respectively for elastic and rigid surfaces

Fig. 8 plots the dimensionless load W versus minimum surface separation $h_{tot,min}$ curves respectively for elastic and rigid surfaces obtained from the present multiscale model for different fluid-bearing surface interactions when u = 1.5E-3 m/s. The slopes of these curves

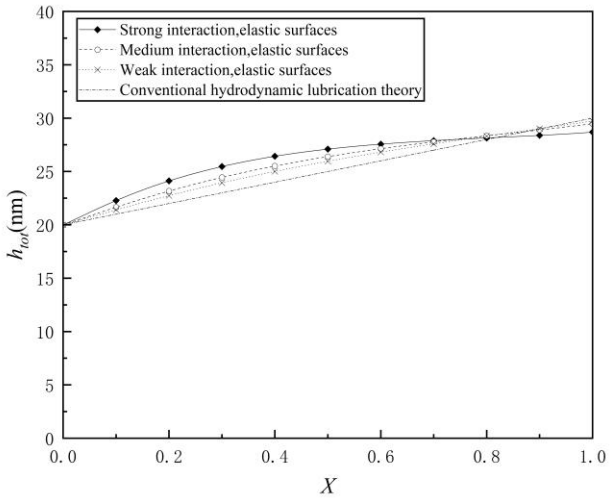

Fig. 6 Comparison of the surface separation profiles for different fluid-bearing surface interactions calculated for elastic surfaces based on the present multiscale model when $h_{tot,min}$ = 20 nm and u = 1.5E-3 m/s

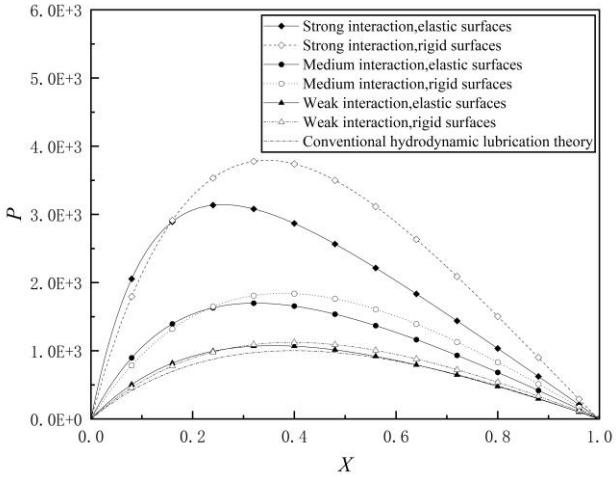

Fig. 7 Comparison of the hydrodynamic pressure profiles calculated respectively for elastic surface and rigid surface based on the present multiscale model when $h_{tot,min}$ = 20 nm and u = 1.5E-3 m/s

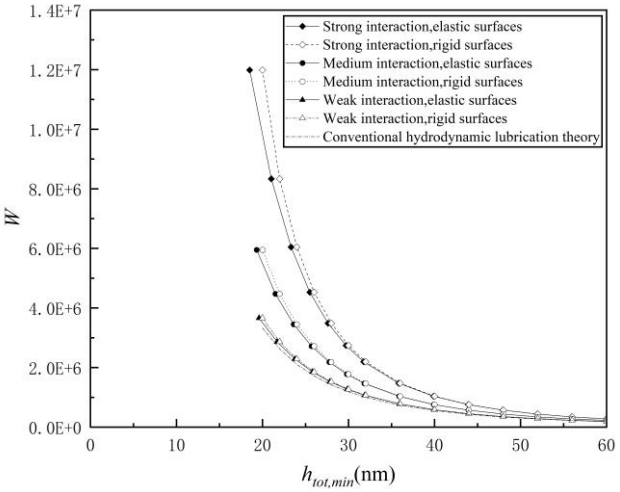

Fig. 8 The load W versus minimum surface separation $h_{tot,min}$ curves respectively for elastic and rigid surfaces obtained from the present multiscale model when u = 1.5E-3 m/s

show the stiffness of the lubricating film in the bearing. It is shown that owing to the effect of the surface elastic deformation, the lubricating film stiffness is reduced especially for a strong fluid-bearing surface interaction and a low value of $h_{tot,min}$. For a given load, the surface elastic deformation results in a smaller value of $h_{tot,min}$; Or for a given $h_{tot,min}$, it results in a smaller load of the bearing. For the present bearing, the surface elastic deformation effect obviously strongly depends on the fluid-bearing surface interaction.

5.3. Operating characteristics of the present bearing owing to the effect of the surface elastic deformation

Fig. 9 shows that the effect of the surface elastic deformation reduces the variation slope of the load of the present bearing with the sliding speed especially for a strong fluid-bearing surface interaction. For a high sliding speed, it may result in a much reduced load of the bearing compared to the calculation result for rigid surfaces.

Fig. 10 shows that for a given load, the increase of the sliding speed raises the whole surface separation whenever the bearing surfaces are elastic or rigid, however the effect of the surface elastic deformation reduces the rate of the increase of the minimum surface separation (at X=0) with the sliding speed compared to the result for rigid surfaces.

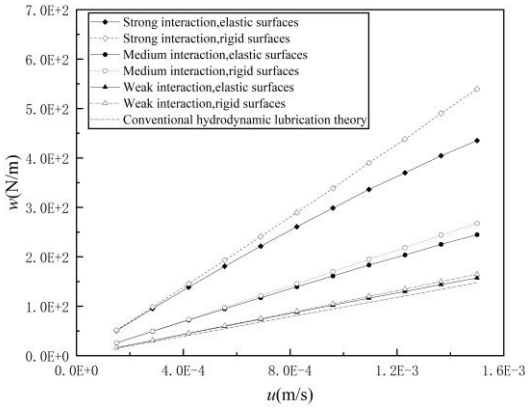

Fig. 9 Dependences of the load of the present bearing on the sliding speed respectively for elastic and rigid surfaces for different fluid-bearing surface interactions when $h_{tot,min}$ = 20 nm

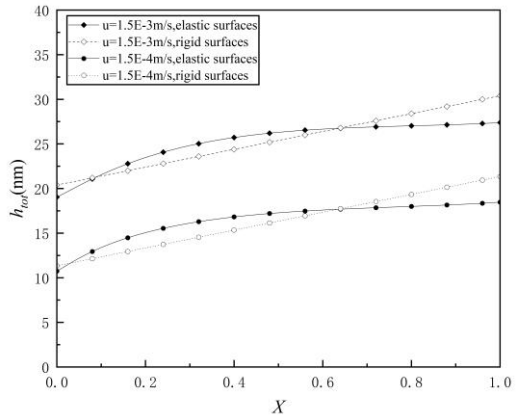

Fig. 10 Influences of the increase of the sliding speed on the surface separation in the present bearing for the strong fluid-bearing surface interaction respectively for elastic and rigid surfaces when w = 500 N/m

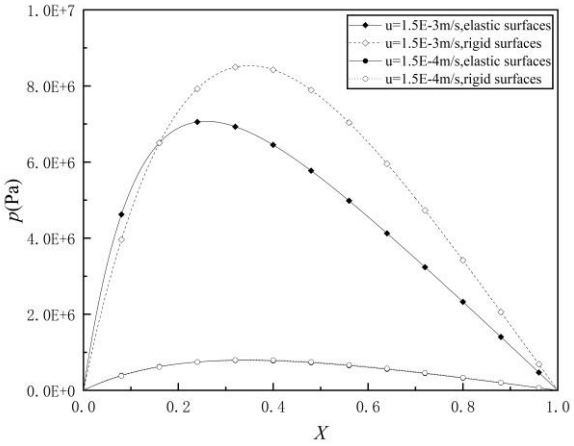

Fig. 11 Influences of the sliding speed on the hydrodynamic pressure in the present bearing for the strong fluid-bearing surface interaction respectively for elastic and rigid surfaces when $h_{tot,min}$ = 20 nm

Fig. 11 shows that for a given $h_{tot,\,min}$, when the effect of the surface elastic deformation is considered, the hydrodynamic pressure in the present bearing is more slowly increased with the increase of the sliding speed, compared to the result for rigid surfaces. When the sliding speed is low enough, the effect of the surface elastic deformation is negligible even for a strong fluid-bearing surface interaction; when the sliding speed is sufficiently high, it greatly reduces the hydrodynamic pressure for a strong fluid-bearing surface interaction.

6. Conclusions

The present study analytically investigates the effect of the surface elastic deformation in the hydrodynamic inclined fixed pad thrust slider bearing with low clearances where both the adsorbed layer flow and the intermediate continuum fluid flow are involved. It was found that the effect of the surface elastic deformation strongly depends on the fluid-bearing surface interaction. For a strong fluid-bearing surface interaction, this effect can be very significant, it can greatly reduce the hydrodynamic pressure and carried load of the bearing for a given minimum surface separation compared to the results for rigid surfaces, and it can also much reduce the increase proportionality of the load of the bearing with the sliding speed compared to that for rigid surfaces. However, when the fluid-bearing surface interaction is weak, the effect of the surface elastic deformation is much weaker and it is often negligible for relatively high surface separations because of low hydrodynamic pressures.

The effect of the surface elastic deformation reduces the lubricating film stiffness. It is particularly significant for a strong fluid-bearing surface interaction and a low minimum surface separation. For a given load, it results in a reduced minimum surface separation compared to that for rigid surfaces. Or for a given minimum surface separation, it results in the load-carrying capacity of the bearing smaller than that for rigid surfaces. When the hydrodynamic pressures in the bearing are sufficiently low in the condition of low sliding speeds, the effect of the surface elastic deformation is negligible even for a strong

fluid-bearing surface interaction. The study indicates the important influence of the surface elastic deformation on the operating characteristics of the present bearing, and suggests the necessity of the incorporation of the effect of the surface elastic deformation in studying the multiscale hydrodynamic thrust slider bearing in the condition of sufficiently high sliding speeds owing to the generated high pressures.

References

1. **Agrawal, N.; Sharma; S. C.** 2023. Micro-grooved hybrid spherical thrust bearing with Non-Newtonian lubricant behaviour, International Journal of Mechanical Sciences 240: 107940. https://doi.org/10.1016/j.ijmecsci.2022.107940.
2. **Williams, P. D.; Symmons, G. R.** 1987. Analysis of hydrodynamic slider thrust bearings lubricated with non-newtonian fluids, Wear 117(1): 91–102. https://doi.org/10.1016/0043-1648(87)90246-8.
3. **Kumar, V.; Sharma, S. C.** 2018. Influence of dimple geometry and micro-roughness orientation on performance of textured hybrid thrust pad bearing, Meccanica 53(14): 3579–3606. https://doi.org/10.1007/s11012-018-0897-0.
4. **Walicka, A.; Walicki, E.; Jurczak, P.; Falicki, J.** 2014. Thrust bearing with rough surfaces lubricated by an ellis fluid, International Journal of Applied Mechanics and Engineering 19(4): 809–822. https://doi.org/10.2478/ijame-2014-0056.
5. **Sternlicht, B.** 1958. Influence of pressure and temperature on oil viscosity in thrust bearings, Journal of Fluids Engineering 80(5): 1108–1112. https://doi.org/10.1115/1.4012622.
6. **Yadav, J. S.; Kapur, V. K.** 1981. On the viscosity variation with temperature and pressure in thrust bearing, International Journal of Engineering Science 19(2): 269–277. https://doi.org/10.1016/0020-7225(81)90027-6.
7. **Karadere, G.** 2010. The effects of the total bearing deformation on the performance of hydrodynamic thrust bearings, Industrial Lubrication and Tribology 62(4): 207–213. https://doi.org/10.1108/00368791011051062.
8. **Güllü, E.** 2005. The effects of bearing distortion on the performance of hydrodynamic thrust bearings, Industrial Lubrication and Tribology 57(3): 121–127. https://doi.org/10.1108/00368790510595093.
9. **Zhai, L.; Luo, Y.; Wang, Z.; Liu, X.; Xiao, Y.** 2017. A review on the large tilting pad thrust bearings in the hydropower units, Renewable and Sustainable Energy Reviews 69: 1182-1198. https://doi.org/10.1016/j.rser.2016.09.140.
10. **Zhang, Y. B.** 2020. Modeling of flow in a very small surface separation, Applied Mathematical Modelling 82: 573-586. https://doi.org/10.1016/j.apm.2020.01.069.
11. **Zhang, Y. B.** 2021. Multiscale hydrodynamics in line contacts, Mechanics Research Communications 111: 103658. https://doi.org/10.1016/j.mechrescom.2021.103658.
12. **Huang, C.; Zhang, Y. B.; Pang, M. J.; Jiang, X. D.** 2020. Multiscale analysis of hydrodynamic inclined fixed pad thrust slider bearing, Journal of the Balkan Tribological Association 27: 243-255.
13. **Atkas, O.; Aluru, N. R.** 2002. A combined continuum/DSMC technique for multiscale analysis of microfluidic filters, Journal of Computational Physics 178(2): 342-372. https://doi.org/10.1006/jcph.2002.7030.
14. **Liu, J.; Chen, S.; Nie, X.; Robbins, M. O.** 2007. A continuum-atomistic simulation of heat transfer in micro- and nano-flows, Journal of Computational Physics 227(1): 279-291. https://doi.org/10.1016/j.jcp.2007.07.014.
15. **Yen, T. H.; Soong, C. Y.; Tzeng, P. Y.** 2007. Hybrid molecular dynamics-continuum simulation for nano/mesoscale channel flows, Microfluidics and Nanofluidics 3(6): 665-675. https://doi.org/10.1007/s10404-007-0154-7.
16. **Zhang, Y. B.** 2004. Modeling of molecularly thin film elastohydrodynamic lubrication, Journal of the Balkan Tribological Association 10: 394-421.
17. **Pinkus, O.; Sternlicht, B.** 1961. Theory of hydrodynamic lubrication, McGraw-Hill, New York.

J. Zhu, Y. Zhang

EFFECT OF SURFACE ELASTIC DEFORMATION IN HYDRODYNAMIC INCLINED FIXED PAD THRUST BEARING WITH LOW CLEARANCE

S u m m a r y

The paper analytically studies the effect of surface elastic deformation in hydrodynamic inclined fixed pad thrust slider bearing with low clearances by the multiscale approach considering the physically adsorbed layer on the bearing surface. The numerical calculation results show that the bearing surface elastic deformation has significant influences on both the hydrodynamic pressure and the surface clearance in the bearing especially for a strong fluid-bearing surface interaction. For given load, sliding speed and bearing geometrical sizes, the surface elastic deformation considerably reduces the minimum bearing clearance, which exists on the exit of the bearing. It also significantly reduces the hydrodynamic film stiffness and the load-carrying capacity of the bearing especially for a strong fluid-bearing surface interaction and low bearing clearances. The increasing proportionality of the carried load of the bearing with the sliding speed is also significantly reduced by the surface elastic deformation particularly for a strong fluid-bearing surface interaction.

Keywords: adsorbed layer, elastic deformation, hydrodynamics, load, pressure, thrust bearing.

Received April 9, 2023
Accepted December 3, 2023